Accepted Manuscript

International Journal of Applied Mechanics

Article Title:	Novel Gradient Design and Simulation of Voronoi Structures
Author(s):	Yang Gu, Xianghong Xu
DOI:	10.1142/S1758825118500795
Received:	03 July 2018
Accepted:	31 July 2018
To be cited as:	Yang Gu, Xianghong Xu, Novel Gradient Design and Simulation of Voronoi Structures, *International Journal of Applied Mechanics*, doi: 10.1142/S1758825118500795
Link to final version:	https://doi.org/10.1142/S1758825118500795

World Scientific
www.worldscientific.com

International Journal of Applied Mechanics

NOVEL GRADIENT DESIGN AND SIMULATION OF VORONOI STRUCTURES

Yang Gu

State Key Laboratory of Nonlinear Mechanics, Institute of Mechanics, Chinese Academy of Sciences, Beijing 100190, People's Republic of China
School of Engineering Sciences, University of Chinese Academy of Sciences, Beijing; Beijing, 100049, P.R.China
guyang@ imech.ac.cn

Xianghong Xu*

State Key Laboratory of Nonlinear Mechanics, Institute of Mechanics, Chinese Academy of Sciences, Beijing 100190, People's Republic of China
xxh@ lnm.imech.ac.cn

The gradient design of a fine grain structure on the surface and coarse grain structure in the substrate gives nano metallic materials both high strength and plasticity. Inspired by the concept of gradient design of grain sizes in materials science, this paper shows the design of the gradient Voronoi polygonal honeycomb structure. The quasi-static uniaxial tensile deformation processes of both, gradient and uniform, Voronoi structures were studied and it was found that the gradient design of the honeycomb cell size greatly improves the tensile property and strain energy storage of the Voronoi structure.

Keywords: *Voronoi structures; gradient design; tensile properties; strain energy storage*

1. Introduction

Natural honeycomb cellular structures such as cork, cancellous bone and the anterior wing of beetles have excellent properties such as low weight, high strength and high energy absorption [Ajdari *et al.*, 2011]. Practical engineering structures such as aerospace vehicles, automobiles and helmets have adopted this cellular porous design to ensure that the high structural strength and energy absorption properties meet the engineering requirements while remaining lightweight [Tang *et al.*, 2016]. In the context of this engineering application, researchers optimized and improved the traditional regular hexagonal honeycomb structures and revealed its deformation mechanism based on the bionic microstructure design to improve the mechanical properties of the porous cellular structure.

On the one hand, under the premise of maintaining the consistency of the material and its relative density, the individual cell morphology of periodic lattice cells can be optimized to improve the structural mechanical properties. In order to reduce the stress concentration at the rigid node of the bar member, Papka and Kyriakides [1994, 1999] designed a circular hole structure at that point in the regular hexagonal honeycomb,

resulting in an increased dynamic equivalent modulus in the optimized structure compared to the static equivalent modulus, thus providing better mechanical properties under dynamic impact loading. Simone and Gibson [1998] introduced a gradient-thickened design at the rigid node, which increased the equivalent elastic modulus of the structure. Shen *et al.* [2013] designed the cell wall thickness gradient to run parallel to the loading direction to increase the energy absorption efficiency of the structure under impact loading. Zhou *et al.* [2017] designed a 2D porous structure with a negative Poisson's ratio by changing the interior angle of the individual cell. The structure is more stable at the plateaued stress zone of the yielding stage under quasi-static uniaxial compression.

On the other hand, non-periodic lattice cells are generated by the Voronoi algorithm and the mechanical properties of Voronoi structures are improved by changing the cellular irregularities between the individual cells. Li *et al*. [2005] believed that the equivalent elastic modulus of Voronoi structures was directly proportional to the degree of cell irregularity and their performance was better than the periodic lattice cellular structure. Sotomayor and Tippur [2014] thought that the reduction in cellular irregularities would flatten the plateau stress of Voronoi structures in the yielding stage; Fazekas *et al.* [2002] revealed that the increase in cellular irregularities would reduce the value of yield stress of Voronoi structures. Thus, in order to achieve optimal mechanical properties, when using the Voronoi algorithm to design porous materials, it is necessary to control the irregularities of individual cells. Furthermore, the gradient design can significantly improve the mechanical properties of materials/structures, which has generated widespread interest in the academic community. Lu *et al.* [2004] and Liu *et al*. [2013] achieved a gradient structure with fine grains on the surface and coarse grains in the substrate by heat-treating the surface of the polycrystalline material. They found that the ductility of the material is improved dramatically by marginally reducing its yield limit, thereby increasing the toughness of the metallic material. Ma and Ye [2007] designed a bilayer structure by combining circular cell elements and hexagonal cell elements, which creates a gradient in the mechanical properties. The energy absorption rate of the bilayer structure under a blast loading was significantly higher than that of the uniform structure. Zhang *et al.* [2016] designed a Voronoi structure with a gradient distribution of member bar material density. The numerical results under impact loading show that the stress at the support end of the density gradient distribution structure increases with increasing impact velocity. Liang *et al.* [2017] introduced a gradient design for the cell size under uniform material density, the positive gradient structure with large cells at the impact end and small cells at the support end yielded excellent energy absorption efficiency and pulse transmission ability under blast loading.

In this paper, a structure similar to gradient nanometals is designed i.e., a Voronoi structure in which the cell size gradient is perpendicular to the loading direction. The deformation characteristics of a uniform and gradient structure under quasi-static uniaxial tension are numerically simulated. The mechanism that leads to a significant increase in the tensile strength and energy absorption of the Voronoi structure with a gradient design

is revealed.

2. Gradient Voronoi model

2.1. Gradient grid random distribution method

A group of cell cores distributed in a 2D region expands outwards in a circular manner at a constant speed within the plane. When adjacent cell walls are in contact, the state of the cell wall is controlled to maintain contact without penetration until the expanded polygons fill this space entirely before the Voronoi polygon structure can be generated. [Zhu *et al.*, 2001].

The total number of cell cores and their spatial distribution are key to controlling the geometry of Voronoi polygons. As shown in Fig.1, N cell cores are distributed in a 2D region of length L_1 and width L_2. If the cell cores are distributed in a uniform manner, a periodically distributed regular hexagonal honeycomb structure can be generated. The distance between two adjacent cell cores is $l_0 = \sqrt{2L_1L_2/(\sqrt{3}N)}$ [Liang *et al.*,2002]. If the cell cores are randomly distributed, the resulting Voronoi structures may have large differences. In order to reduce the individual differences of Voronoi polygons, Martinez and Martinez [2002] proposed the concept of inhibition distance, which assumes that the minimum distance between cell cores is λl_0, where $0 < \lambda < 1$. As the value of λ increases, the cell core distribution becomes more ordered. When $\lambda = 0$, the inhibition distance method does not work, and the cell cores are completely randomly distributed; when $\lambda = 1$, the cell cores are arranged in a periodic lattice. With a given value of λ, the cell cores can be randomly distributed in the 2D region. When the distance between the newly distributed cell core and the existing cell core is less than λl_0, the newly distributed cell core does not meet the requirements and has to be redistributed until N cell cores are obtained. The inhibition distance method can achieve a statistically uniform distribution of cell size in the whole region.

In order to achieve the non-uniform design of cell size distribution in Voronoi model, a gradient grid random distribution method is proposed in this paper. First, the 2D area is divided into I layers and each layer is divided into a specific number of grids, the number of grids in the i-th layer is given by $J_i (i = 1, 2, \cdots I)$, so the grid length is,

$$l_{1i} = \frac{L_1}{J_i} \tag{1.1}$$

The width of the model is equal to the sum of grid widths of all I layers, i.e., $L_2 = \sum_{i=1}^{I} l_{2i}$. Suppose all the grids have the same length-width ratio $\psi = l_{1i}/l_{2i}$, and then,

$$\psi = \frac{L_1 \sum_{i=1}^{I} (1/J_i)}{L_2} \qquad \psi = \frac{L_1 \sum_{i=1}^{I} (1/J_i)}{L_2} \tag{1.2}$$

Following this, one cell core is randomly distributed in each grid so that the number of cell cores in the i-th later is the same as the number of grids, J_i. The total number of cell cores is given by $N=\sum_{i=1} J_i$. The resulting Voronoi polygons has no limitation of minimum distance between cell cores. Moreover, assuming, J_i satisfies,

$$J_i = INT[a_0 - a(i - (I+1)/2)^2] \tag{1.3}$$

where INT is the integral function, a_0 is the undetermined constant, a is the gradient coefficient which representing the gradient of cell size along the y-axis. Finally, all the edges of the generated Voronoi polygon are translated in-plane to obtain member bars of the same thickness and a Voronoi solid model can be obtained. The numerical model is then generated by assigning the same cross-sectional properties to all cell boundaries. The relative density of the Voronoi model can be obtained by dividing the sum of the areas of all bars by the area of the 2D region. When calculating the total area of the bars, if the thickness of the bar is much smaller than its length, then the high-order small areas of the rigid connections of the bars can be ignored, and the member bars at the edge of the model can be excluded. With a given relative density, model length $L_1$and width L_2, total number of cell cores N, grid layer I and gradient coefficient a, then cell core number of each layer J_i, grid sizes l_{1i} and l_{2i}, and cell wall thickness b can be uniquely determined.

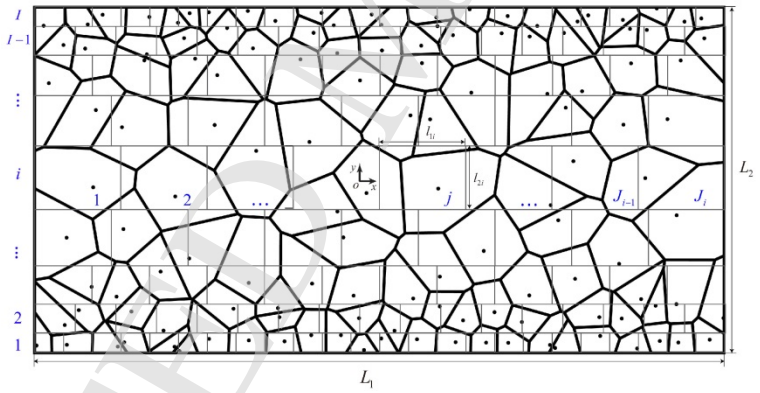

Fig. 1. Gradient grid random distribution method for generating Voronoi polygons. The coordinate origin O is located at the center of the model, and x and y represent the length and width of the model, respectively; the thin solid lines are the grid edges, the dots and thick solid lines are the cell cores and edges, respectively; L1 and L2 are the length and width of the model, respectively; I is the layer number of grids, J_i, l_{1i} and l_{2i} are the grid number, length and width of the i-th grid layer, respectively.

Figure 2(a) shows the distribution curve of the number of cell cores J_i along the grid layer. The corresponding Voronoi model is shown in Fig. 3. The relative density was 0.3 %, the length of the model L_1= 200, the width L_2= 60 mm, the thickness of out-plane was 20 mm, the total number of cell cores $N=2000\pm10$, the grid layer$I=35$. The 18th layer is the central layer and J_i is symmetrical about it. When the gradient coefficient, $a=0$, J_i is constant and the number of cell cores in each layer is the same; when $a<0$,

the number of cell cores on the upper and lower edges is greater than that of cell cores near the center; when $a>0$, the number of cell cores on the upper and lower edges is smaller than the number closer to the center. The distribution of J_i along the *y*-direction is uniquely determined by *a*; the larger the absolute value of *a*, the larger the gradient change in the number of cell cores. In order to avoid the cells with serious shape distortion, the value of *a* is set between -0.4 and 0.2.

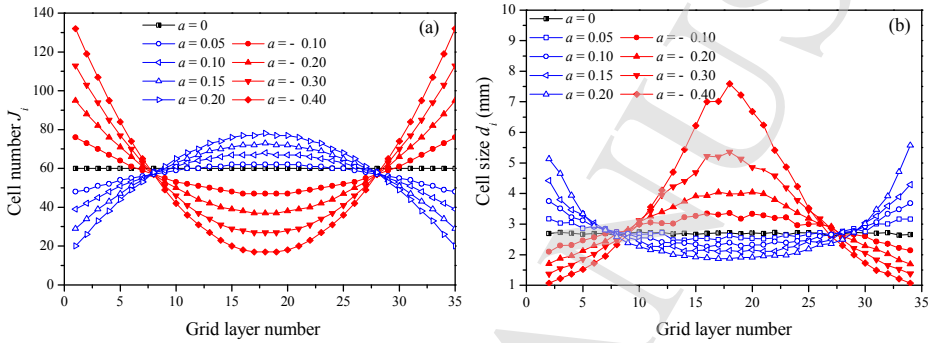

Fig.2. Distribution curves of (a) the number of cell cores J_i and (b) the average cell size in a layer d_i along the grid layer. The total cell number N = 2000 ± 10, the grid layer number I = 35, and the gradient coefficient a is between -0.4 and 0.2.

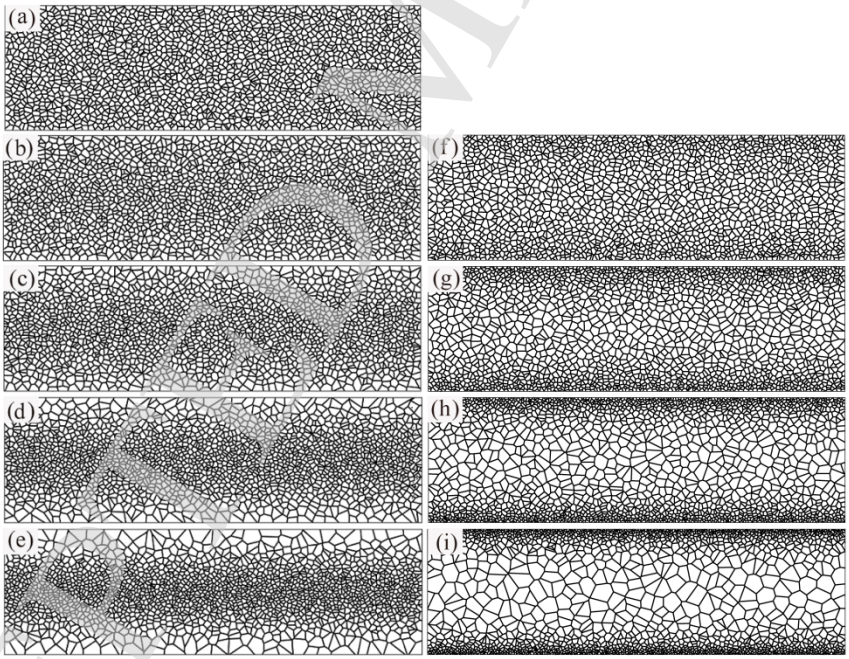

Fig.3. Voronoi models with the gradient coefficient a = (a) 0; (b) 0.05; (c) 0.10; (d) 0.15; (e) 0.20; (f) - 0.1; (g) - 0.2; (h) - 0.3; (i) - 0.4. The relative density is about 0.3 %.

2.2. *Evaluation parameters for the gradient Voronoi model*

The differences in the shapes and sizes of the uniform model cells are statistically uniform throughout the area. The difference in cell shapes of the gradient model is statistically uniform in the entire region; however, the difference in cell sizes is made up of two components – the difference in average cell size between layers and the difference in cell sizes within the same layer. The former is determined by the gradient coefficient and the latter is equivalent to the uniform model. Therefore, on the one hand, the difference in cell shapes of the gradient model can be characterized by the method used for cell shape difference in the uniform model as specified in the existing literature [Tang *et al*., 2014], and the cell shape distortion can be characterized by the sum of the relative angular differences between the Voronoi K polygon and the regular K polygon,

$$\theta_{ij} = \sum_{k=1}^{K} \frac{|\theta_k - \theta_0|}{\theta_0} \tag{2.1}$$

where θ_k is the value of the interior angle in row i and column j of the Voronoi K polygon, and θ_0 is the value of the interior angle of the regular K polygon. The mean, R_{shape}, and variance, D_{shape}, of the shape distortion of the gradient model can be written separately as,

$$R_{\text{shape}} = \frac{\sum_{i=2}^{I-1}\sum_{j=2}^{J_i-1}\theta_{ij}}{\sum_{i=2}^{I-1}(J_i - 2)} \tag{2.2}$$

$$D_{\text{shape}} = \sqrt{\frac{\sum_{i=2}^{I-1}\sum_{j=2}^{J_i-1}(\theta_{ij} - R_{\text{shape}})^2}{\sum_{i=2}^{I-1}(J_i - 2)}} \tag{2.3}$$

On the other hand, the difference in the cell sizes of the gradient model is determined after removing the inter-layer cell difference caused by the gradient coefficient. The relative difference between the cell sizes of the Voronoi polygon and average cell sizes in the same layer is used to characterize the difference in cell sizes,

$$e_{ij} = \frac{|d_{ij} - d_i|}{d_i} \tag{2.4}$$

where d_{ij} is the cell size of the polygon in the i-th row and the j-th column, i.e. the diameter of a circle with an area equivalent to the area of the polygon; $d_i = \frac{1}{n_i - 2}\sum_{j=2}^{n_i-1} d_{ij}$ is the average of all polygon cell sizes in the i-th layer. The mean, $R_{¿¿¿}$, and the standard deviation, $D_{¿¿¿}$, of the cell size difference in the gradient model can be written as,

$$R_{\text{size}} = \frac{\sum_{i=2}^{I-1}\sum_{j=2}^{J_i-1}e_{ij}}{(I - 2)\times(J_i - 2)} \tag{2.5}$$

$$D_{\text{size}} = \sqrt{\frac{\sum_{i=2}^{I-1}\sum_{j=2}^{J_i-1}\left(e_{ij} - R_{\text{size}}\right)^2}{\sum_{i=2}^{I-1}\left(J_i - 2\right)}} \tag{2.6}$$

Considering that the generated Voronoi structure is in a finite 2D rectangular area, the cells that intersect the boundary are cropped out, hence not included in the statistical analysis. Therefore, only cells from layer 2 to layer $I-1$ and from column 2 to column $(J¿¿i-1)(i=1,2,\ldots I)¿$ are counted in Eqs. (5), (6), (8), and (9). Figure 2(b) shows the change in the average cell size in a layer d_i with the number of grid layers. d_i is also approximately symmetrically distributed about the center layer. For simplicity, the following description of the gradient $\frac{d_i}{y}$ of the cell size along the *y*-direction is for the upper half of the model; that is for layers 18 to 35 (y ≥ 0) . When the gradient coefficient, $a=0$, the average cell size in a layer d_i does not change in the *y*-direction and the cell size gradient, $\frac{d_i}{y}0$; when $a<0$, the cell sizes have a negative gradient, which decreases from the center to the edge, and $\frac{d_i}{y}<0$; when $a>0$, the cell sizes have a positive gradient, which increases from the center to the edge, and $\frac{d_i}{y}>0$. It can be seen that the change in gradient of the cell sizes along the *y*-direction, $\frac{d_i}{y}$, is uniquely determined by the gradient coefficient, *a*, and the larger the absolute value of a, the greater the absolute value of $\frac{d_i}{y}$, which means that the trend of change in cell size becomes more dramatic.

Based on the gradient grid random distribution method, the cell cores are randomly distributed within the grid. Thus, although the number of cell cores J_i is uniquely determined, the generated Voronoi polygons corresponding to the same gradient coefficient, a, are different due to the different positions of the cell cores in the grid, i.e., any value of a corresponds to multiple gradient models. Figure 4 shows the statistical distribution of the mean and variance of the Voronoi model's cell size difference and shape distortion. The number of samples for any value of a is 10,000. The statistical distributions of $R_{¿,D_{¿¿¿}¿}$, R_{shape} and D_{shape} at different values of a satisfy the Gaussian function. The fitting parameters are shown in Table 1. When |a| increases (i.e., the cell size gradient $¿\frac{d_i}{y}\vee ¿$ increases), the mean value μ and the standard deviation φ of the cell size differences and shape distortions show an increasing trend. To make the investigated model more representative, four quality assessment parameters will be selected in the model in the range of $\mu \pm 2\varphi$ when calibrated.

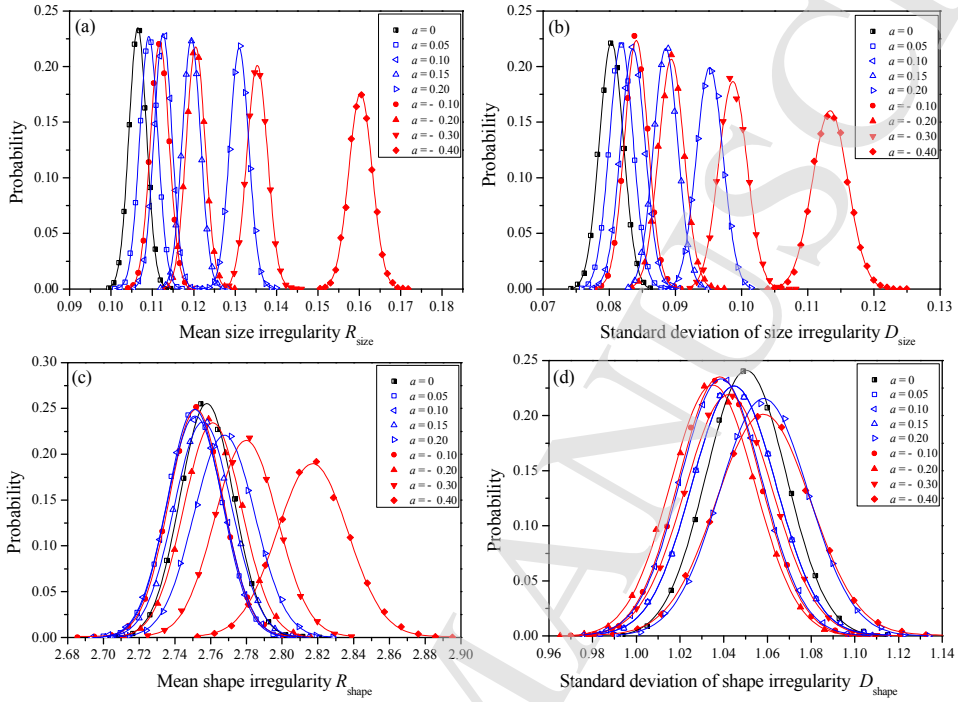

Fig.4. Statistical distributions of: (a) Rsize; (b) Dsize; (c) Rshape; (d) Dshape.

Table 1 Evaluation parameters of the Voronoi models

Gradient coefficient a	Size irregularity				Shape irregularity			
	R_{size}		D_{size}		R_{shape}		D_{shape}	
	$\mu/10^{-1}$	$\varphi/10^{-3}$	$\mu/10^{-2}$	$\varphi/10^{-3}$	μ	$\varphi/10^{-2}$	μ	$\varphi/10^{-2}$
0.00	1.06	2.11	8.03	1.81	2.76	1.49	1.05	1.84
0.05	1.09	2.19	8.18	1.80	2.75	1.52	1.04	1.92
0.10	1.13	2.17	8.36	1.84	2.74	1.57	1.04	1.88
0.15	1.19	2.23	8.85	1.84	2.76	1.61	1.05	1.92
0.20	1.31	2.30	9.52	2.02	2.77	1.71	1.06	2.04
- 0.10	1.12	2.26	8.41	1.77	2.75	1.50	1.04	1.87
- 0.20	1.20	2.28	8.94	1.93	2.76	1.62	1.03	1.93
- 0.30	1.35	2.49	9.87	2.15	2.78	1.75	1.04	2.00
- 0.40	1.60	2.83	11.3	2.70	2.82	1.98	1.06	2.16

3. Finite element model

The quasi-static uniaxial stretching process of the Voronoi model was numerically simulated using the finite element software Abaqus. The internal bar of the model is made of Al5052-H39 [Gibson and Michael, 1999], which has a density of 2750 kg/m^2.

The bilinear post-hardening elastoplastic constitutive model is adopted, and the corresponding constitutive curve is shown in Fig.5(a). The elastic modulus is 68.97 GPa, and the Poisson's ratio is 0.32; the initial yield stress is 282 MPa, and the shear modulus is 0.69 GPa; the plastic strain limit is 0.287. When the strain exceeds this value, the stress will remain constant at 480 MPa.

As the porous structure is under tensile loading, the boundaries members will occurs large deformation and support most external load if with the same material properties as the internal ones. However, the surface of real materials is uneven, usually contains microholes and other defects, and will not dominate the properties of the whole structure. Therefore, the upper and lower edge members are supposed to be made of rubber materials to weaken the boundary effect, and the Mooney-Rivlin hyperelastic model is used in the analysis [Mooney, 1940]. When the nominal strain reaches 300%, the nominal stress of the material reaches a maximum of 1.22 MPa, and the corresponding constitutive curve is shown in Fig.5(b).

The left edge member of the model is a rigid body with a fixed boundary condition; the right edge member is also a rigid body, but with a displacement boundary condition applied.

The quasi-static loading is applied along the *x*-direction. Timoshenko beam element B22H is used. B22H is a plane beam element using three nodes and hybrid elements, which can simulate the stretching and bending of the lower beam section with large deformations.

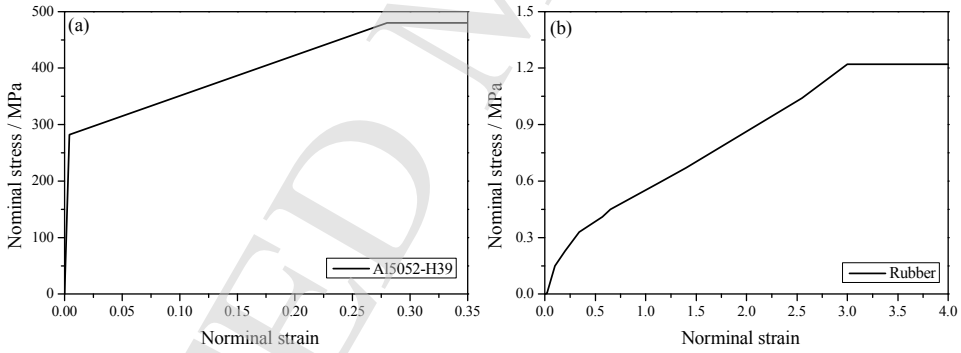

Fig.5. Stress-strain curve of (a) Al5052-H39, (b) Rubber for the simulation.

4. Results

Figure 6 shows the nominal stress - strain curves of the Voronoi model under uniaxial tension with different gradient coefficients. As the nominal strain increases, the nominal stress increases exponentially. Under the same nominal strain, the percentage increment of the nominal stress of the gradient model is used to quantitatively characterize the increase rate of its tensile property compared to the nominal stress of the uniform structure. Under nominal strains, ε = 4%, 6%, and 8%, the growth rate of the tensile property of the gradient model with corresponding changes in the gradient coefficient is

shown in Fig. 7. The number of samples in each case is 10. When the relative density, the total number of cells and the number of grid layers are the same, the gradient coefficient a has a significant effect on the tensile strength of the structure. In comparison with a uniform structure with randomly uniform distributed cell sizes ($a0$), the gradient structure with a non-uniform cell size distribution ($a0$) exhibits significantly improved tensile property. With an increase in the absolute value of a, the cell size gradient is larger, and the growth rate of the tensile property of the gradient structure is higher. For the negative gradient structure where a = - 0.4 and the positive gradient structure where a = 0.2, the maximum increase percentage of tensile property are 70.5% and 44.4% respectively.

Meanwhile, under the same nominal strain, the strain energy stored in the gradient structure is also higher than that stored in the uniform structure. When ε = 8%, the strain energy stored in two gradient structures with a = - 0.4 and 0.2 is 70.5% and 34.8% higher than that of the uniform structure respectively, as shown as in Fig.8. When $\varepsilon \leq 8$ %, the elastic strain energy of the three groups of distributed models exceeds the total energy stored in the structure during its elastic deformation stage by 98.2%.

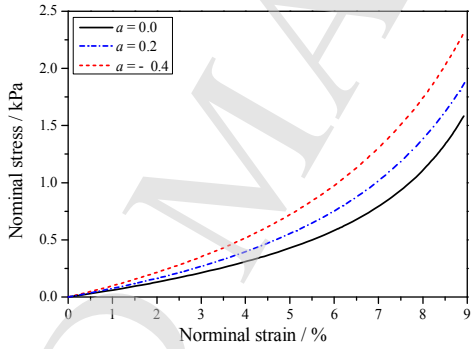

Fig.6. Nominal stress-strain curves of Voronoi models under quasi-static uniaxial tension.

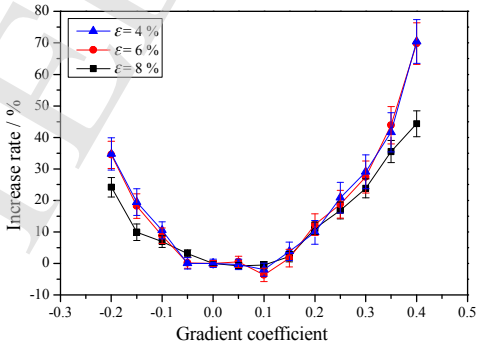

Fig.7. Increase rate of the tensile property of the gradient model with different gradient coefficient.

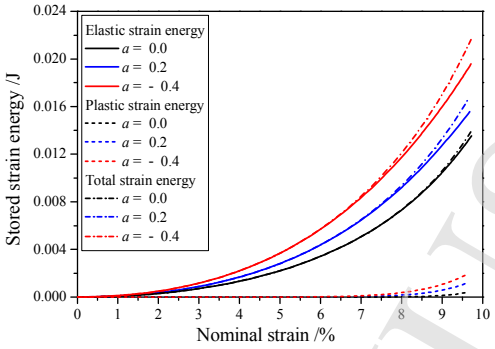

Fig.8. Strain energy stored in Voronoi structure under quasi-static uniaxial tension.

The Voronoi model is a porous structure consisting of a series of bars of different lengths, as shown as in Fig.9(a). The member bar acts as a load-bearing component. During the loading process, the strain energy concentration zone is located at the node or midpoint of the member bar (Fig. 9(b)). The area of strain energy concentration of the uniform Voronoi model is randomly and uniformly distributed throughout the structure, and the area of the strain energy concentration of the gradient model is concentrated in the dense parts of the bars, as shown in Fig.10. With an increase in nominal strain, the strain energy concentration zone increases and the strain energy in the concentrated area also increases. The area of strain energy concentration of the uniform model gradually spreads over the entire area. In the gradient model, the area of strain energy concentration tends to converge at the denser areas of the bars

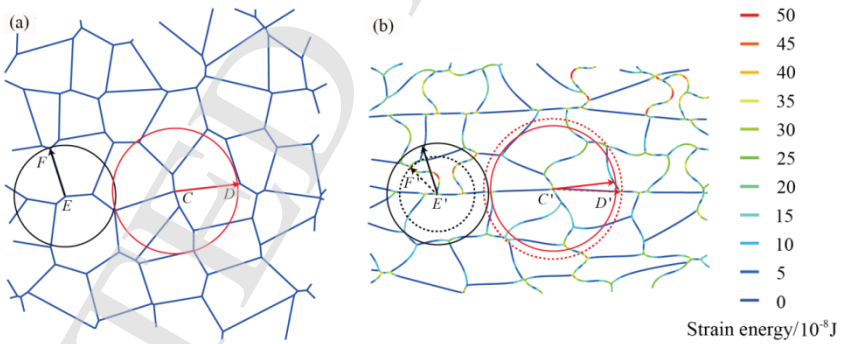

Fig.9. Construction diagrams of the bar prior to and after loading with (a) Initial state; (b) deformed state. C′D′ and E′F′ refer to bars CD and EF post deformation, and the solid circular radius and dashed circular radius represent the respective straight-line distances between the two ends of the bar before and after deformation.

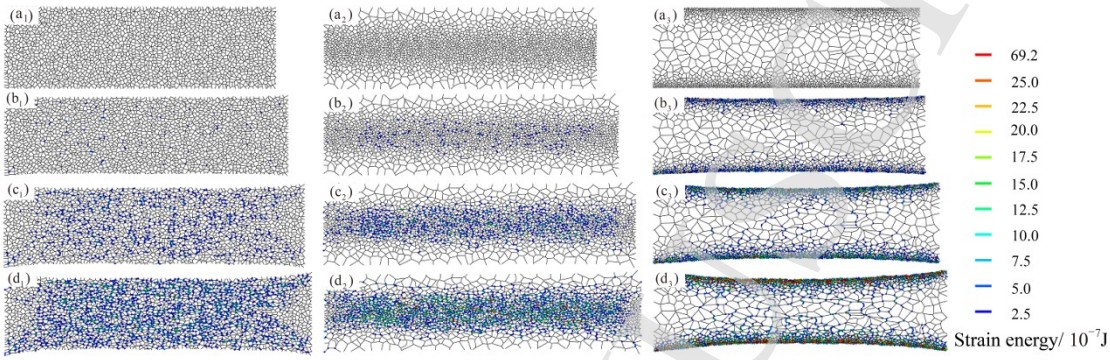

Fig.10. Evolution of strain energy distribution of the Voronoi structure with the gradient coefficient (a1)-(d1) 0, (a2)-(d2) 0.2, (a3)-(d3) -0.4 at the nomial strain (a1)-(a3) 2%, (b1)-(b3) 4%, (c1)-(c3) 6%, (d1)-(d3) 8%.

Figure 11 shows the distribution of the mass of the bar along each grid layer of the different Voronoi structures. The mass of all the member bars in each layer was calculated, and the uniform structure with an average value of masses of all bars except the two edge layers 1 and 35 is used for nondimensionalization to obtain the dimensionless mass of the layer. For a uniform structure, the bars are randomly distributed, and the total mass of the bars in each layer is almost equal (symbol ◨ in Fig. 11). At any stage of loading, the stored strain energy in each layer is also nearly equal and will increase as the structure deforms, as shown in Fig.12(a). For the gradient structure, the mass of the bar of each layer is different (symbols □ and ■ in Fig. 11). In the initial stage of loading, the elastic strain energy absorbed by each layer is almost equal; as the structural deformation increases, the difference in stored strain energy between the layers increases, and the strain energy stored by the mass concentration layer of the bar increases sharply. Furthermore, the larger the value of nominal strain, the greater the proportion of strain energy stored by the bar in areas of high concentration, as shown in Figs. 12(b) and (c). The mass of the bars towards the central area of the positive gradient is greater than that near the edges, and the stored strain energy is mainly concentrated in the middle of the structure; conversely, the mass of the bars in the middle of the structure with a negative gradient is smaller than that at the edges, and the strain energy is mainly concentrated in the upper and lower edges of the structure. Therefore, under constant relative density, the gradient design of the cell size of the model can determine the redistribution of location and size of strain energy concentration and improve the energy storage and tensile performance of the overall structure.

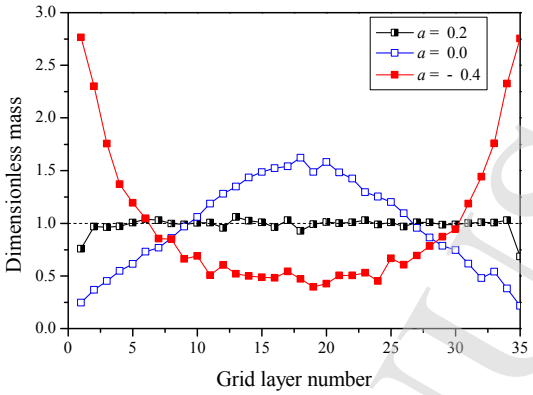

Fig.11. Distribution of the dimensionless mass of the bars along each grid layer.

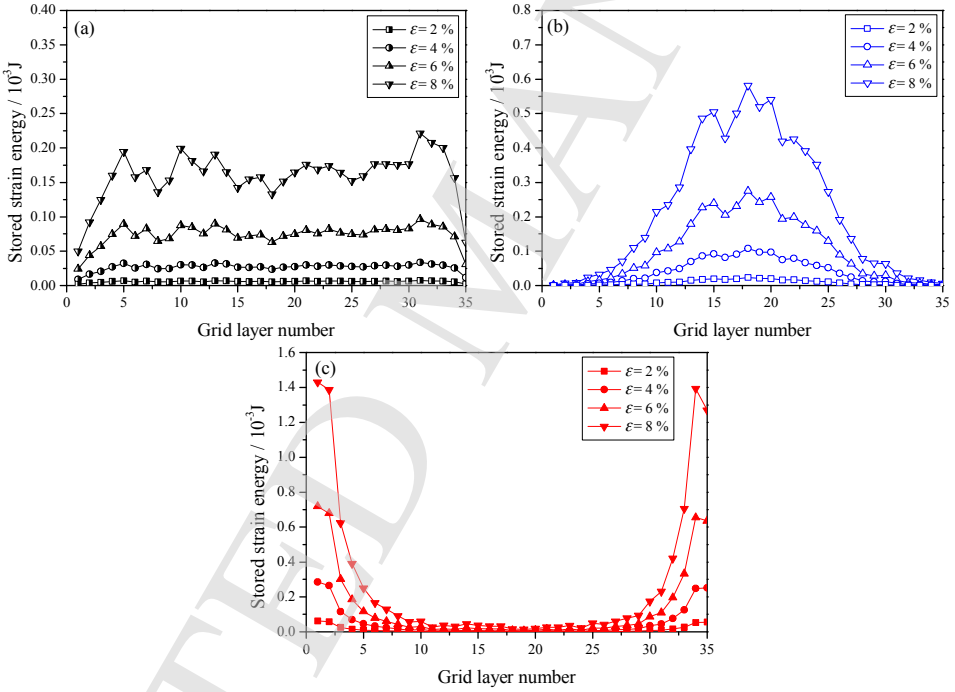

Fig.12. Evolution of stored strain energy in each layer of the Voronoi with gradient coefficient (a) 0, (b) 0.2, (c) -0.4.

Moreover, the force, deformation and energy storage of the bars under the uniaxial tension are analyzed. Figure 13(a) shows the basic structural unit of the Voronoi model, and the node P and the bars in three different directions intersecting at this node; Q, Q_1 and Q_2 are the midpoints of the bars and the length of bar PQ is l_a, its angle to the x-axis is α and the width in the y-direction of the structural unit is l_b. When the model is in quasi-static uniaxial tension, its basic structural unit is in static equilibrium, which can be simplified as both sides are subjected to tensile stress σ_1 in the x direction, as shown in

Fig. 13(b).

Static analysis is performed on member bar *PQ*. The internal force in section *Q* is an axial tensile force $\sigma_1 l_b L_3 cos\alpha$, the shear force is $\sigma_1 l_b L_3 sin\alpha$ and the bending moment is $\sigma_1 l_a l_b L_3 sin\alpha/2$. Therefore, the deformation modes of the bars in a Voronoi model under uniaxial tension include axial tension, bending and shear. In the initial stage of loading, the deformation of the bar is small and satisfies the assumption of small deformation. The elastic strain energy stored in *PQ* has three components: axial tension, bending and shear strain energy,

$$U=\int_0^{l_a}\frac{(\sigma_1 l_b L_3 cos\alpha)^2}{2EA}dx+\int_0^{l_a}\frac{\left(x\sigma_1 l_b L_3 sin\alpha-\frac{\sigma_1 l_a l_b L_3 sin\alpha}{2}\right)^2}{2EI}dx+\int_0^{l_a}\frac{3(\sigma_1 l_b L_3 sin\alpha)^2}{5GA}dx \tag{4.1}$$

where the tensile stiffness $EA=b L_3$, the bending stiffness $EI=L_3 b^3/12$, the shear modulus $G = E/2(1+\nu)$, and ν is Poisson's ratio. As the axial force and shear force remain unchanged along the axis direction of the bar, Eq. (19) can be integrated into,

$$U=\frac{L_3 l_a l_b^2 \sigma_1^2}{2Eb}\left(\cos^2\alpha+\frac{l_a^2\sin^2\alpha}{b^2}+\frac{12\sin^2\alpha(1+\nu)}{5}\right) \tag{4.2}$$

Under axial tension, the axis of the bar will remain straight; when a bending moment/shear force is applied, the axis of the bar will bend. Under the continuous action of the load, the deformation of the bar will gradually increase, and the assumption of small deformation no longer applies. Figure 9 shows the construction diagrams of the bar prior to and after loading. C′D′ and E′F′ refer to bars CD and EF post deformation, and the solid circular radius and dashed circular radius represent the respective straight-line distances between the two ends of the bar before and after deformation. Any two nodes in the model are rigidly connected by bars. When the member bar is loaded axially, the member bar extends and the distance between the two nodes increases; when the member bar is subject to a shear force or a bending moment, the distance between the two nodes will decrease. Before loading, lines CD and EF are straight. After loading, line C′D′ is approximately straight and its straight-line distance is larger than that at the initial state, which indicates that C′D′ is dominated by tensile deformation; E′F′ is a curve, and its straight-line distance is smaller than that at the initial state, indicating that E′F′ is dominated by bending deformation. This shows that the change in the distance between the two ends of the bar corresponds to the main deformation mode of the bar. The bar with the two-end distance increased is defined as the bar dominated by tensile deformation and is simply called a tensile bar; the bar with the two-end distance decreased is defined as the bar dominated by bending deformation and is simply called a bending bar.

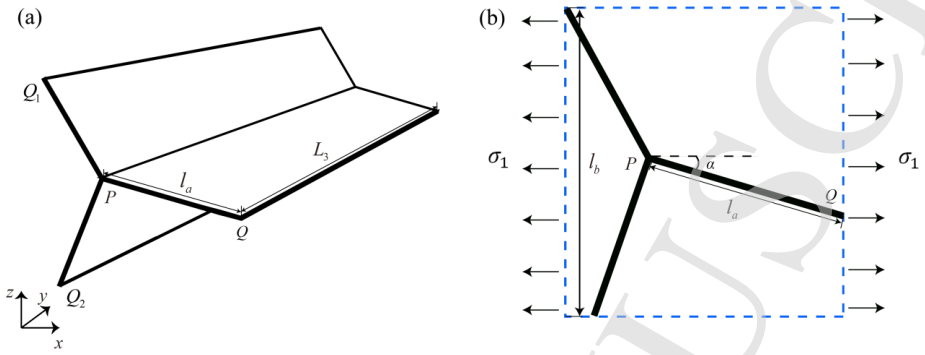

Fig.13. Basic structural unit of the Voronoi model with (a) 3D side view and (b) 2D force analysis diagram, which includes the node P and the bars in three different directions intersecting at this node; Q, Q_1 and Q_2 are the midpoints of the bars and the length of bar PQ is l_a, its angle to the x-axis is α and the width in the y-direction of the structural unit is l_b.

Regardless of uniform distribution or gradient distribution of cell sizes, in the case where the relative densities are the same, i.e. the total mass of the bar is the same, as shown in Fig.14, the ratio of the mass of the bending bar to the total mass of the gradient structure is very close to that of the uniform structure, and the ratios of total strain energy absorbed by the bending bar to the total strain energy of the structures are also close to. At any stage of loading, the total mass of the bending bar is much greater than the total mass of the tensile bar. At the initial stage of loading, the total mass of the bending bar accounts for more than 85% of the total mass of the structure. As the structural deformation increases, this proportion slowly increases, and will exceed 95% when the nominal strain is 8% (dashed lines in Fig. 14). Furthermore, the strain energy absorbed by the bending bar in the structure is much higher than that of the tensile bar, which dominates the structural absorption strain energy. At the initial stage of loading, the strain energy absorbed by the bending bar accounts for more than 89% of the strain energy absorbed by the structure. As the structural deformation increases, this proportion increases slowly and exceeds 98% at a nominal strain of 8% (solid lines in Fig. 14).

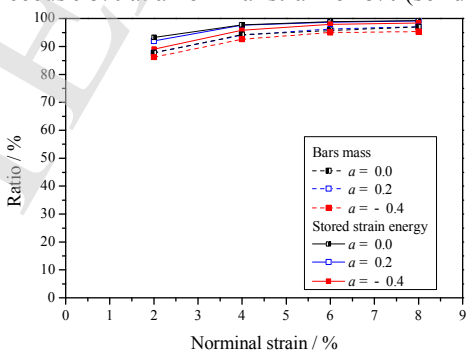

Fig.14. Ratios of the mass of the bending bars to the total mass and the strain energy absorbed in the bending to the total absorbed energy.

The spatial distribution of the mass of the gradient Voronoi structure exhibits non-

uniformity and there is an apparent area of mass concentration in the member. At the center of the positive gradient structure, the mass of the layer member bar is approximately 1.65 times that of the uniform structure. Similarly, at the edges of the negative gradient structure, the mass of the layer member bar is approximately 2.81 times that of the uniform structure, as shown in Fig.11. Under the same axial nominal strain, the transverse necking of the negative gradient structure is obvious, and the transverse deformation of the positive gradient structure and the uniform structure is small, as shown in Fig.10. During tensile loading, necking is observed in the structure and lateral deformation in the upper and lower edges is greater than that observed towards the center of the structure. Therefore, the strain energy stored in the multi-row bar layer at the edges is significantly larger than that stored in the densely arranged bar layer at the center. Moreover, as the density of the bar increases, the amount of extrusion at both ends of the bar also increases and the bending deformation of the bar increases, this leads to the increase of the strain energy stored in the bar. The stored bending strain energies at the center of the positive gradient structure and at the edges of the negative gradient structure are 3.45 and 8.24 times that of the uniform structure respectively, as shown in Fig.15. Because of this non-uniform arrangement, the total strain energy stored in the positive and negative gradient structures are 1.4 and 1.82 times that stored in the uniform structure, as shown in Fig.16. Thus, the performance of the overall structure under tensile loading is greatly improved.

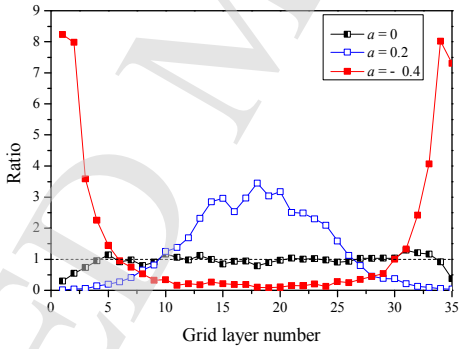

Fig.15. Ratios of the stored strain energy in bending bars of gradient Voronoi structure to that of uniform structure at nominal strain of 8 %.

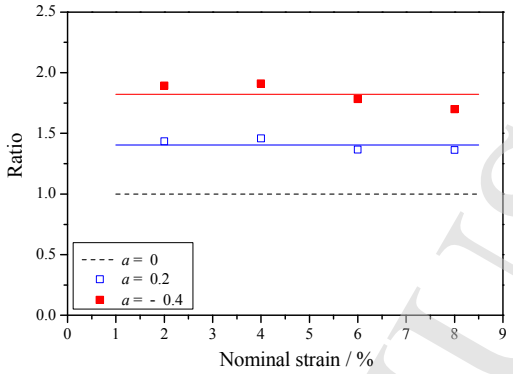

Fig.16. Ratios of the total stored strain energy in gradient structure to uniform structure.

5. Conclusions

(1) A gradient grid random distribution method for generating Voronoi polygons is proposed to achieve a non-uniform design of the cell size in the entire model area. Voronoi structures in which the cell sizes are uniformly distributed along the width of the model are generated when the gradient coefficient is 0. Similarly, structures in which the cell sizes show a gradient distribution are obtained when the gradient coefficient is non-zero.

(2) By using the relative difference in the cell size and average cell size in the same layer, the difference in cell size in the Voronoi gradient model is defined. The difference caused by cell size gradient is eliminated, which makes the degree of difference in the cell sizes of different Voronoi structures comparable.

(3) When the relative densities are equal, the uniaxial tensile properties of the gradient Voronoi structure are better than those of the uniform structure, the gradient coefficient increases, its enhancement effect is more apparent and the tensile property of the structure with smaller cell sizes on the upper and lower edges increases. The tensile property of the gradient structure can be 70.5% higher than that of the uniform structure.

(4) The mass of the bar is arranged non-uniformly perpendicular to the direction of tensile loading, which causes greater deformation and bending in areas of greater concentration of mass and increase in the stored strain energy. This is the main reason why the gradient structure with a relatively consistent density can store 1.82 times the strain energy stored in a uniform structure.

Acknowledgments

The authors are grateful for the support from the National Natural Science Foundation of China (No. 11672297) , and the Strategic Priority Research Program of the Chinese Academy of Sciences (No. XDB22020200).

References

Ajdari, A., Nayeb-Hashemi, H and Vaziri, A. [2011] "Dynamic crushing and energy absorption of regular, irregular and functionally graded cellular structures," *International Journal of Solids and Structures* **48**(3-4), 506-516.

Fazekas, A., Dendievel, R and Salvo, L. [2002] "Effect of microstructural topology upon the stiffness and strength of 2D cellular structures," *International Journal of Mechanical Sciences* **44**(10), 2047-2066.

Gibson, L and Michael, F. A. [1999] *Cellular Solids: Structure and Properties* (Cambridge university press., Cambridge).

Liang, M. Z., Li, Z. B and Lu, F. Y. [2017] "Theoretical and numerical investigation of blast responses of continuous-density graded cellular materials," *Composite Structures* **164**, 170-179.

Li, K., Gao, X. L and Subhash, G. [2005] "Effects of cell shape and cell wall thickness variations on the elastic properties of two-dimenional cellular solids," *International Journal of Solids and Structures* **42**(5-6), 1777-1795.

Liu, X. C., Zhang H. W and Lu, K. [2013] "Strain-Induced ultrahard and ultrastable nanolaminated structure in nickel," *Scicence* **342**(6156), 337-340.

Lu, L., Shen, Y. F and Chen, X. H. [2004] "Ultrahigh strength and high electrical conductivity in copper," *Science* **304**(5669), 422-426.

Ma, G. W and Ye, Z. Q. [2007] "Energy absorption of double-layer foam cladding for blast alleviation," *International Journal of Impact Engineering* **34**(2), 329-347.

Martinez, W. L and Martinez, A. R. [2002] *Computational Statistics Handbook with MATLAB* (Chapman & Hall/CRC., Boca Raton).

Mooney, M. [1940] "A theory of large elastic deformation," *Journal of applied physics* **11**(9), 582-592.

Papka, S. D and Kyriakides, S. [1994] "In-plane compressive response and crushing of honeycomb," J*ournal of the Mechanics and Physics of Solids* **42**(10), 1499-1532.

Papka, S. D and Kyriakides, S. [1999] "Biaxial crushing of honeycombs: —Part 1: Experiments," International Journal of Solids and Structures **36**(29), 4367-4396.

Papka, S. D and Kyriakides, S. [1999] "In-plane biaxial crushing of honeycombs—: Part II: Analysis," International Journal of Solids and Structures **36**(29), 4397-4423.

Shen, C. J., Lu, G. and Yu, T. X. [2013] "Dynamic behavior of graded honeycombs - A finite element study," *Composite Structures* **98**, 282-293.

Simone, A. E and Gibson, L. J. [1998] "Effects of solid distribution on the stiffness and strength of metallic foams," *Acta Materialia* **46**(6), 2139-2150.

Sotomayor, O. E and Tippur, H. V. [2014] "Role of cell regularity and relative density on elasto-plastic compression response of random honeycombs generated using Voronoi diagrams," *International Journal of Solids and Structures* **51**(21-22), 3776-3786.

Tang, H. P., Wang, Q. B and Yang, G. Y. [2016] "A Honeycomb-Structured Ti-6Al-4V Oil–Gas Separation Rotor Additively Manufactured by Selective Electron Beam Melting for Aero-engine Applications," *JOM* **68**(3), 799-805.

Tang, L. Q., Shi, X. P and Zhang, L. [2014] "Effects of statistics of cell's size and shape

irregularity on mechanical properties of 2D and 3D Voronoi foams," *Acta Mechanica* **255**(4-5), 1361-1372.

Zhang, J. J., Wang, Z. H and Zhao, L. M. [2016] "Dynamic response of functionally graded cellular materials based on the Voronoi model," *Composites Part B* **85**, 176-187.

Zhou, Z. X., Zhou, J. N and Fan, H. L. [2017] "Plastic analyses of thin-walled steel honeycombs with re-entrant deformation style," *Materials Science and Engineering: A-structural materials properties microstructure and processing* **688**, 123-133.

Zhu, H. X., Hobdell, J. R and Windle, A. H. [2001] "Effects of cell irregularity on the elastic properties of 2D Voronoi honeycombs," *Journal of mechanics and physics of solids* **49**(4), 857-870.